scientific reports

Check for updates

OPEN

Sequential game dynamics produce subgame perfect equilibria in sports networks through bounded rationality

Chulwook Park[1,2,3]✉

Strategic decision-making in networked systems unfolds sequentially, with each agent's choice shaped by the observable actions of those who decide earlier. We extend bounded rationality from simultaneous to sequential decision structures on scale-free networks, showing how modified backward induction yields approximate subgame perfect equilibria that converge to their exact counterparts as the rationality parameter increases, forming bounded-rationality refinements of Nash equilibria. Agents ordered by network centrality condition on their predecessors' actions through a centrality-weighted observation term, with social learning and strategic exploration jointly defining a behavioral regime that ranges from winner-takes-all configurations concentrated among hub agents to broader participation with flattened centrality gradients. In the four equilibrium scenarios examined, the sequential protection distribution stochastically dominates the simultaneous baseline, and centrality-based ordering outperforms random and inverse alternatives. Cross-domain calibration against banking, epidemiological, and sports network data shows that introducing the observation term strengthens the centrality–protection correlation in all three domains, consistent with a common mechanism operating across distinct behavioral systems.

Keywords Sequential game theory, Subgame perfect equilibrium, Bounded rationality, Scale-free sports networks, Centrality-based decision ordering

Complex sports systems present a distinctive class of strategic interactions. Agents, whether individual athletes, functional units, or teams, decide sequentially, observing and responding to predecessors' actions within interconnected network structures[1–4]. Both simultaneous formulations and asynchronous updating have informed network-game studies, including our own demonstration that Nash equilibria emerge from bounded rationality in simultaneous sports networks[5]. Centrality-ordered sequential play with explicit observation of predecessors has received less systematic attention as a route to equilibrium selection on scale-free networks.

Sequential strategic interactions in sports networks

In reality, strategic adaptation in sports follows sequential patterns, where teams observe rivals' tactical innovations before responding, athletes adjust techniques after witnessing competitors' performances, and coaching decisions cascade through organizational hierarchies[6,7]. The sequential nature of sports competition is not merely incidental but structurally fundamental to strategic outcomes. Championship series in professional baseball, basketball, and hockey are paradigmatic sequential games. Two teams play a sequence of contests, and each game's outcome alters the strategic landscape for subsequent games, creating state-dependent incentive structures that simultaneous models cannot capture[8]. In these settings, game trees map the evolving state space and backward induction identifies the subgame perfect equilibrium (SPE), the solution concept that requires optimal play in every possible continuation of the game.

Ferrall and Smith[8] formalized this structure for best-of-n championship series, solving the SPE and estimating its parameters across three professional sports using data from World Series (1922–1993), NBA Finals (1955–1994), and Stanley Cup Finals (1939–1994). Beyond multi-game series, sequential structure pervades sports at finer scales. In penalty shootouts, kickers and goalkeepers adjust strategies based on earlier

[1]Department of Physical Education, Seoul National University, Seoul, South Korea. [2]Complexity Science and Evolution, Okinawa Institute of Science and Technology (OIST), Okinawa, Japan. [3]Systemic Risk and Resilience, International Institute for Applied Systems Analysis (IIASA), Laxenburg, Austria. ✉email: pcw8531@snu.ac.kr

outcomes. In football, offensive play selection, run versus pass and formation choice, triggers defensive counter-adjustments in real time. In baseball, batting order construction reflects sequential considerations, where each lineup position faces a different game state. These examples share three defining characteristics of sequential games. First, decisions occur in a specific temporal order. Second, agents possess information about predecessors' actions. Third, optimal strategies are determined by thinking ahead through backward induction rather than through simultaneous best-response calculation.

These sequential models in sports, however, have remained dyadic. Rosen[9] analyzed how elimination tournament structures require escalating prizes to sustain effort incentives across sequential rounds, while Lazear and Rosen[10] established that rank-order compensation schemes can replicate the efficiency of piece-rate contracts when monitoring is costly. Ferrall and Smith's[8] subgame perfect equilibrium analysis is confined to two contestants or a single hierarchical ladder. Our contribution extends sequential game logic from these dyadic contests to multi-agent networked systems, where the decision ordering is determined endogenously by network centrality rather than by an external schedule, and where bounded rationality replaces the assumption of perfect strategic calculation.

Game-theoretic foundations and the sequential refinement

Game theory provides the foundational mathematical basis for analyzing strategic interactions among rational decision-makers[11,12]. A finite noncooperative game is defined by the tuple (N, S, U), where N is the set of players, $S = S_i$ is the Cartesian product of each player's action set, and $U = (U_i, \ldots, U_n)$ is the vector of payoff functions. A strategy profile s^* constitutes a Nash equilibrium (NE) when no player can unilaterally deviate to improve their payoff[12]:

$$U^A\left(S^{A*}, S^{B*}\right) \geq U^A\left(x, S^{B*}\right) \text{ and } U^B\left(S^{A*}, S^{B*}\right) \geq U^B\left(S^{A*}, y\right) \tag{1}$$

for every pure strategy x of player A and every pure strategy y of player B. Nash's seminal existence theorem establishes that every finite game possesses at least one equilibrium in mixed strategies[12,13]. The proof proceeds through Kakutani's fixed point theorem[13]. Player i's mixed strategy σ_i is a probability distribution over pure strategy set S_i. The mixed strategy set is defined as:

$$\Sigma_i = \{\sigma_i = (\sigma_i(s_i), \ldots, \sigma_i(s_k)) \mid 0 \leq \sigma_i(s_k) \leq 1, \Sigma_k \sigma_i(s_k) = 1\} \tag{2}$$

The best response correspondence for player i is defined as:

$$\mathrm{BR}_i(\sigma_i) = \left\{\sigma_i \in \Sigma_i \mid u_i(\sigma_i, \sigma_i) \geq u_i\left(\sigma'_i, \sigma_i\right), \forall \sigma'_i \in \Sigma_i\right\} \tag{3}$$

The combined best response correspondence $\mathrm{B} = (\mathrm{BR}_1, \mathrm{BR}_2) : \Sigma_1 \times \Sigma_2 \to \Sigma_1 \times \Sigma_2$ satisfies four conditions, namely (i) the domain and codomain $\Sigma_1 \times \Sigma_2$ is compact and convex, (ii) for any $\sigma_i \in \Sigma_i$ the best response $\mathrm{BR}_i(\sigma_i)$ is non-empty, (iii) the best response correspondence is convex-valued, and (iv) the correspondence is upper hemi-continuous (closed graph). By Kakutani's fixed point theorem[13], B possesses at least one fixed point $\sigma^* \in B(\sigma^*)$, which satisfies:

$$\sigma_1^* \in \mathrm{BR}_1(\sigma_2^*) \text{ and } \sigma_2^* \in \mathrm{BR}_2(\sigma_1^*) \tag{4}$$

This fixed point constitutes the mutual best response mixed strategy Nash equilibrium $\sigma^* = (\sigma_1^*, \sigma_2^*)$ (Fig. 1). In team sports, such strategic interactions are embedded in interaction networks whose structure shapes team performance[14].

However, when strategic interactions unfold sequentially, the appropriate solution concept shifts from NE to SPE. The extensive form representation of sequential games was formalized by Kuhn[15], who established the equivalence of mixed and behavioral strategies under perfect recall, providing the structural foundation on which Selten[16] introduced the SPE refinement. The relationship between rationality assumptions and equilibrium outcomes is central to this transition. Classical decision theory characterizes risk attitudes through the concavity of the Bernoulli utility function $u(y)$, where concave u corresponds to risk aversion, linear u to risk neutrality, and convex u to risk loving[17,18]. The formal treatment, including Jensen's inequality and the Arrow-Pratt risk aversion measures that connect these utility properties to the softmax parameter β in our model, is developed in SI Text S3.

Bounded rationality and the present study

Under bounded rationality, agents do not perform exhaustive utility calculations but instead rely on heuristic processes including social learning and strategic exploration[5,19,20]. Three established approaches modify classical backward induction to accommodate imperfect strategic reasoning. Quantal response equilibrium (QRE) replaces deterministic best responses with probabilistic choice proportional to expected payoffs, using a logit specification whose precision parameter controls the degree of rationality[21]. McKelvey and Palfrey[22] extended QRE to extensive form games through the agent quantal response equilibrium, which imposes a statistical version of sequential rationality and yields a unique selection from the set of subgame perfect equilibria in generic games. Cognitive hierarchy theory[23] posits that players reason with heterogeneous depths of strategic thinking, where step- k thinkers best-respond to a believed distribution of lower-step opponents. Our softmax-modified backward induction (Eq. 12 below) draws on the QRE tradition, in which the rationality parameter beta plays the same role as the QRE precision parameter, while the social learning and exploration mechanisms (p_r, p_e) from our published model[5] provide the network-specific adaptation process absent in standard QRE

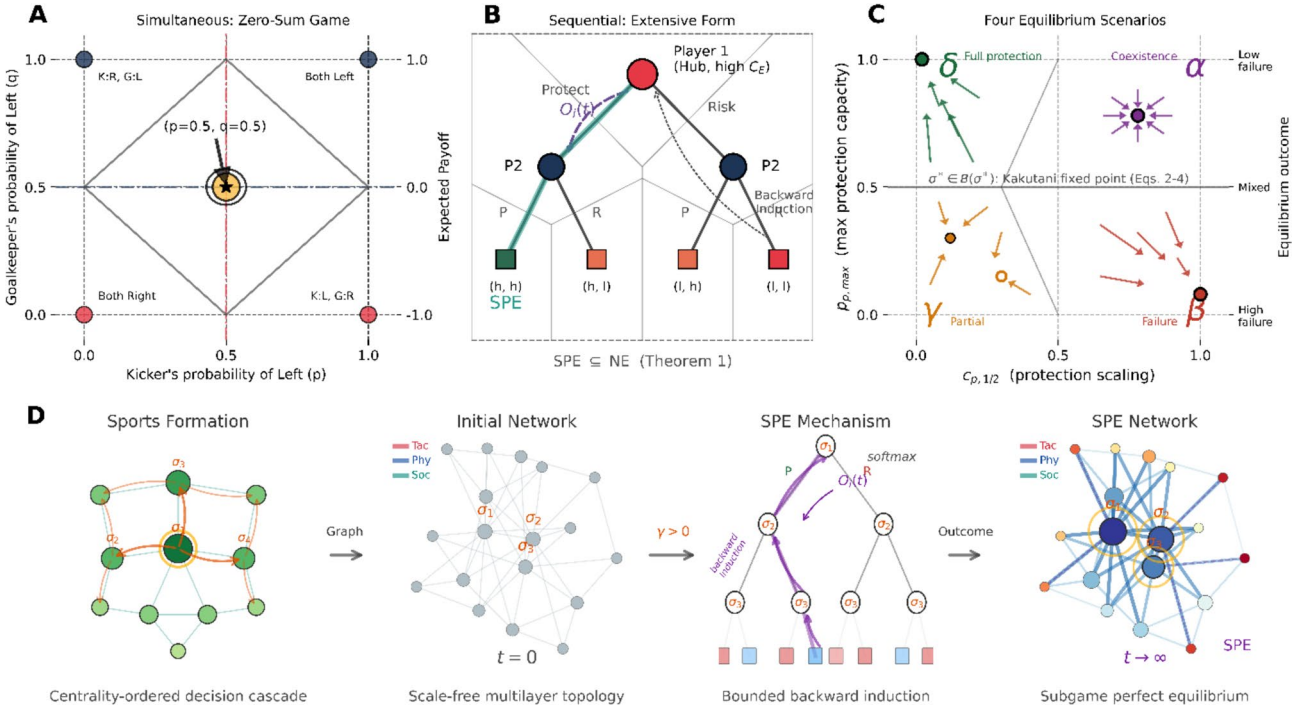

Fig. 1. Strategic interactions and network structure in sports systems. (**A**) Simultaneous zero-sum game. Mixed strategy Nash equilibrium at ($p = 0.5,\ q = 0.5$) for the penalty kick game, where regions partition the strategy space around equilibrium (Eq. 1). (**B**) Sequential extensive form game. Centrality-based decision ordering $\sigma\ (i)$ determines that high- C_E hub nodes move first, with later movers observing predecessors' actions through $O_i\ (t)$; the subgame perfect equilibrium (SPE) path is identified via backward induction, satisfying SPE $\subseteq$ NE (Theorem 1). (**C**) Four equilibrium scenarios (α : coexistence, β : system failure, γ : partial coexistence, δ : full protection) emerging from the interaction between p_{pmax} and $c_{p,1/2}$, with the fixed point $\sigma^* \in B(\sigma^*)$ guaranteed by Kakutani's theorem (Eqs. 2–4). (**D**) Schematic flow from sports context to equilibrium outcome. Left: abstract team formation (4-3-3) with centrality-ordered decision cascade, where the hub node (σ_1, gold ring) initiates sequential observation that propagates outward to peripheral agents (σ_2– σ_4). Center-left: initial scale-free network (i.e., Tactical, Physiological, and Social layers) at $t = 0$ with uniform undifferentiated states. Center-right, SPE mechanism via bounded backward induction with softmax action selection. The game tree shows protection (P) vs. risk (R) decisions at each σ -ordered stage, with the $O_i\ (t)$ observation term enabling later movers to condition on predecessors' actions. Right: the same network at $t \to \infty$ showing centrality-differentiated subgame perfect equilibrium, where hub nodes (high C_E, early movers) achieve protected states while peripheral nodes exhibit heterogeneous failure-protection outcomes through the $\gamma > 0$ sequential observation channel.

and cognitive hierarchy treatments. When these processes operate within sequential structures, agents use imperfect backward reasoning combined with observational learning, producing a modified form of backward induction that converges to approximate SPE. The inclusion of subgame perfect equilibria within the Nash set is a standard relationship from extensive-form refinement theory[15,16], whereas the existence and convergence of ϵ -subgame perfect equilibria are proven in this work (SI Text S2), and the first-order stochastic dominance of the sequential protection distribution over the simultaneous baseline across the four scenarios is reported as a model-based numerical finding (Fig. 4). The novelty of our approach lies in embedding QRE-type probabilistic choice within a network setting where social learning and strategic exploration drive equilibrium emergence, a combination absent from the existing sequential game literature on sports.

Our previous work demonstrated that Nash equilibria emerge from bounded rationality in simultaneous games on scale-free networks, identifying four distinct equilibrium scenarios determined by the interplay between maximum protection capacity (p_{pmax}) and combined failure-propagation risk[5]. A complementary analysis has further demonstrated that network centrality drives optimal protection investment in scale-free networks, establishing that nodes with higher eigenvector centrality invest proportionally more in protection through social learning and centrality-based heuristics[24]. The present study extends this approach to sequential game structures, addressing three fundamental questions, namely (i) Do subgame perfect equilibria emerge from bounded backward induction in networked agents? (ii) How does the temporal ordering of decisions, determined by network centrality, affect equilibrium selection compared to simultaneous play? (iii) Under what conditions do sequential and simultaneous game structures produce equivalent versus distinct equilibrium outcomes?

Results

Sequential game structure on scale-free networks

The extensive form game is constructed on Barabási–Albert networks with $N = 100$ nodes and connectivity $m = 5$. Agents are ordered by eigenvector centrality C_E (Eq. 8), with the most central agents moving first according to the decision order $\sigma(i)$ (Eq. 9). Each agent observes the protection decisions of all predecessors before choosing their own strategy, creating a perfect information sequential game where later movers incorporate predecessors' actions through the centrality-weighted observation term $O_i(t)$ (Eq. 15b). The sequential protection function $f_p(t) = s_i^0 + s_i^1 \cdot C_E(v_i) + \gamma \cdot O_i(t)$ augments the simultaneous model with $\gamma = 0.3$, producing a modified backward induction process in which social learning (p_r) and strategic exploration (p_e) operate within the sequential ordering rather than in parallel (Table 1). Four parameter regimes, defined by the balance between maximum protection capacity (p_{pmax}) and the protection scaling constant ($c_{p,1/2}$), are examined under this sequential structure to characterize how centrality-based decision ordering shapes equilibrium outcomes (Fig. 2). The four scenarios under sequential play preserve the qualitative equilibrium classification established under simultaneous play[5] while exposing structural features unique to the sequential setting.

In each panel, the three-layer network progression shows how the sequential mechanism transforms system dynamics. At t_1, all agents begin from identical initial conditions without scale-free differentiation. At t_2, the observation term $O_i(t)$ introduces asymmetric information as later-moving agents adjust their protection investments based on the centrality-weighted actions of predecessors. By t_3, the SPE under bounded rationality exhibits clear hub-dominated structure where high-centrality early movers anchor the strategic landscape. The best response diagrams confirm that the equilibrium protection level varies systematically across scenarios, from near-zero crossing in Scenario B (insufficient protection capacity prevents any effective strategic response) to high- q crossing in Scenario D (robust protection enables strong mutual best responses). Critically, Scenarios A and C produce coexistence equilibria analogous to mixed strategies, whereas Scenarios B and D correspond to corner outcomes where protection either universally fails or universally succeeds. These patterns indicate that the sequential observation mechanism refines rather than disrupts the equilibrium structure, consistent with the theoretical relationship SPE(Γ) $\subseteq$ NE(Γ) established in Theorem 1 (Eq. 18). The degree to which sequential play produces equilibria distinct from simultaneous play is examined systematically in the following section through direct comparison across the full parameter space.

Modified backward induction under bounded rationality

The equilibrium scenarios established in the preceding section emerge from the interaction between protection capacity (p_{pmax}) and protection scaling ($c_{p,1/2}$), with failure propagation held constant. We now examine how neighbor-contagion risk (p_l) reshapes the equilibrium landscape and how introducing sequential observation through the parameter γ (Eq. 16) transforms these equilibria.

The ternary flow fields (Fig. 3A) trace the progressive effect of increasing failure propagation probability on system composition at fixed γ = 0.3. At low contagion (p_l = 0.1, A1), the attractor sits near the protection vertex with predominantly healthy network nodes and hub-protected topology. As p_l increases through moderate values (A2, A3), the attractor migrates toward a balanced mixed state and embedded networks show spreading failure among peripheral nodes. At high contagion (A4, A5), the attractor approaches the failure cascade vertex, embedded networks show cascading hub failures characteristic of scale-free topology, and protection investment alone cannot contain propagation. This progression establishes the failure-propagation axis that complements the protection-capacity axis examined in Fig. 2. Together, p_{pmax}, $c_{p,1/2}$, and p_l define the three-dimensional parameter space within which sequential observation operates. Under simultaneous play (Fig. 3B), the Nash

Symbol	Parameter	Range	Function in the model
N	Network size	∈ [100, 500]	Sets network scale; ordering and threshold robust across the range (Fig. S3)
m	Connectivity	∈ [2, 5]	Builds the scale-free topology used throughout
p_{pmax}	Maximum protection	∈ [0.1, 1.0]	With $c_{p,1/2}$, defines the four equilibrium scenarios (Fig. 2)
$c_{p,1/2}$	Saturation constant	∈ [0.1, 1.0]	With p_{pmax}, defines the four equilibrium scenarios (Fig. 2)
p_r	Imitation rate	∈ [0.01, 0.99]	With p_e, sets variance reduction and the behavioral regime (Figs. 3C and 6)
p_e	Exploration rate	∈ [0.01, 0.99]	With p_r, sets the regime, lowered to 0.001 for long runs (Fig. 4E)
β	Rationality	∈ [0.1, 50.0]	Sharpens softmax choice, higher β drives ε-SPE toward exact SPE (Eq. 11)
γ	Observation weight	∈ [0, 1.0]	Sequential observation strength, drives refinement and dominance (Figs. 3D and 4)
p_n	Node failure	∈ [0.1, 0.5]	Baseline failure origination, held fixed across scenarios
p_l	Link contagion	∈ [0.1, 0.5]	Swept to trace the failure-propagation axis (Fig. 3A)

Table 1. Core simulation parameters. Core simulation parameters, their explored ranges, and their role in the analyses. The four-scenario analyses (Figs. 2, 3 and 4) fix m= 5, γ = 0.3, and p_n= 0.1, and use T= 100 over 50 realizations. The centrality-dependent fate selection (Fig. 4E) uses T= 50,000 over 3 realizations with p_e= 0.001. The state variables that these parameters act on, centrality, protection, failure, and capacity, are mapped to the empirical observables of each domain in SI Table S2, and the cross-domain calibration appears in Fig. 5. Full operational ranges are given in SI Table S6. All parameters reduce to the published simultaneous model when γ = 0.

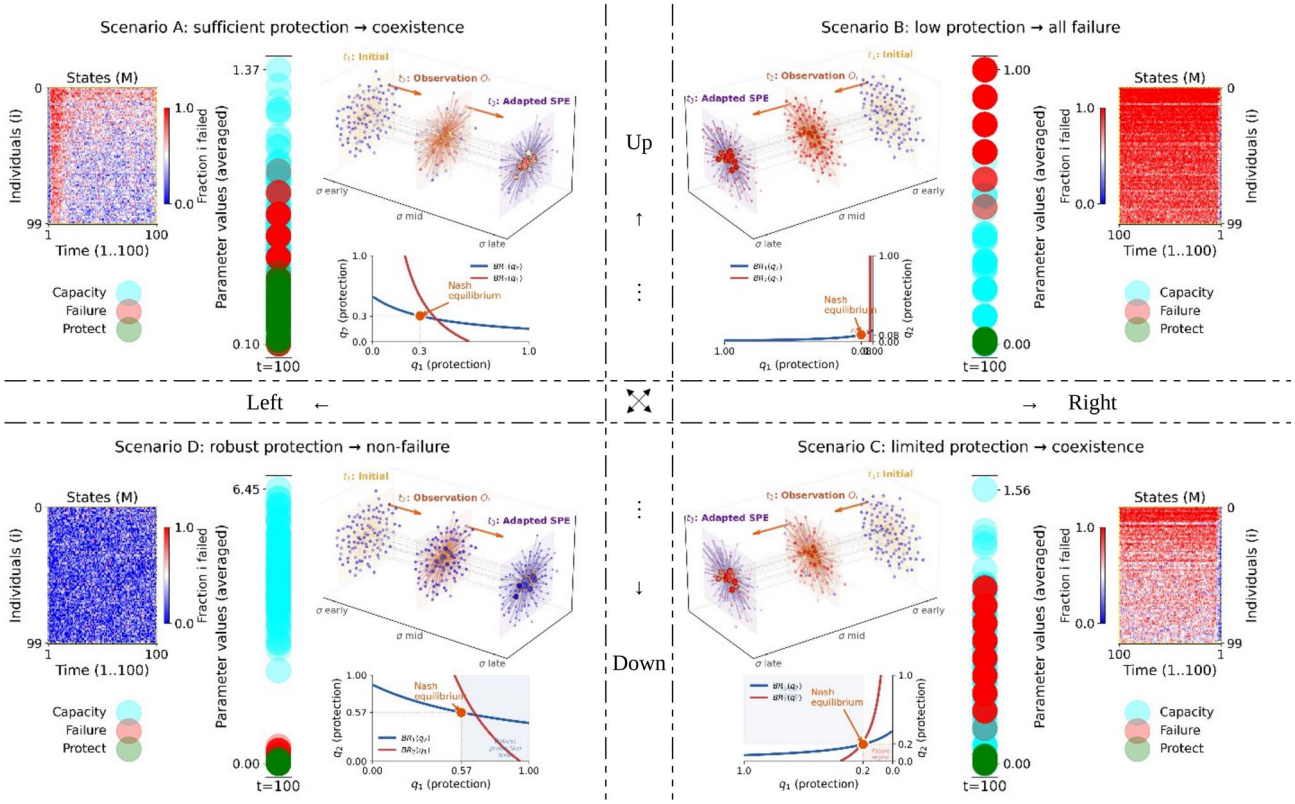

Fig. 2. Four protection–failure equilibrium scenarios under sequential structure. Each panel shows the state matrix (time steps 1–100, nodes 1–100; failure in red, nonfailure in blue, averaged over 10 realizations); three-layer sequential progression on the scale-free network (t_1: initial uniform state, t_2: observation O_i emerging, t_3: adapted SPE with hub dominance); scatter plot of functional capacity (cyan), failure (red), and protection (green) at $t = 100$; and best response diagram with $\mathrm{BR}_1(q_2)$ and $\mathrm{BR}_2(q_1)$ curves intersecting at Nash equilibrium. Parameters: $N = 100$, $m = 5$, $p_n = 0.1$, $\gamma = 0.3$, $\sigma(i)$ by C_E. Scenario A (upper left): sufficient protection ($p_{pmax} = 1.0$, $c_{p,1/2} = 1.0$) yields stable coexistence. Scenario B (upper right): low protection ($p_{pmax} = 0.1$, $c_{p,1/2} = 1.0$) produces system-wide failure. Scenario C (lower right): limited protection ($p_{pmax} = 0.1$, $c_{p,1/2} = 0.1$) generates red-dominant partial coexistence with surviving clusters. Scenario D (lower left): robust protection ($p_{pmax} = 1.0$, $c_{p,1/2} = 0.1$) achieves near-complete non-failure.

equilibrium lies at approximately (q_1, q_2) ≈ (0.35, 0.35), the unique fixed point where neither agent benefits from unilateral deviation. When $\gamma = 0$, agents decide simultaneously and the model exactly reproduces the published Nash equilibrium results[5]. When $\gamma > 0$, later-moving agents observe predecessors' protection strategies before choosing their own, enabling modified backward induction that refines the equilibrium set. Introducing sequential observation (Fig. 3D) shifts the best-response intersection to a new SPE location requiring higher protection from early movers, consistent with the observation advantage that later-moving agents exploit through the γ -weighted alignment term. The faded NE reference and refinement arrow in Panel D confirm SPE ⊂ NE as predicted by Proposition 2.

The refinement landscape (Fig. 3C) quantifies this tightening across the learning parameter space. Variance reduction is strongest when both social learning (p_r) and exploration (p_e) are high. Among the four scenarios, the full protection regime (δ) achieves peak refinement, the all-failure regime (β) remains trapped regardless of sequential structure, and the coexistence scenarios (α , γ) show intermediate refinement, with γ exhibiting a distinctive two-attractor saddle that reflects competing equilibrium basins under limited protection capacity. The central question addressed in the following section is how the sequential observation weight γ controls equilibrium selection across these regimes, and whether centrality-based ordering generates stochastic dominance over simultaneous play.

Sequential dominance and ordering effects

Under sequential decision-making ($\gamma = 0.3$) with centrality-based move ordering (Eq. 9), the sequential protection distribution first-order stochastically dominates the simultaneous baseline in all four scenarios examined in our simulations:

$$F_{seq}(y) \leq F_{sim}(y) \quad \forall\, y \tag{5a}$$

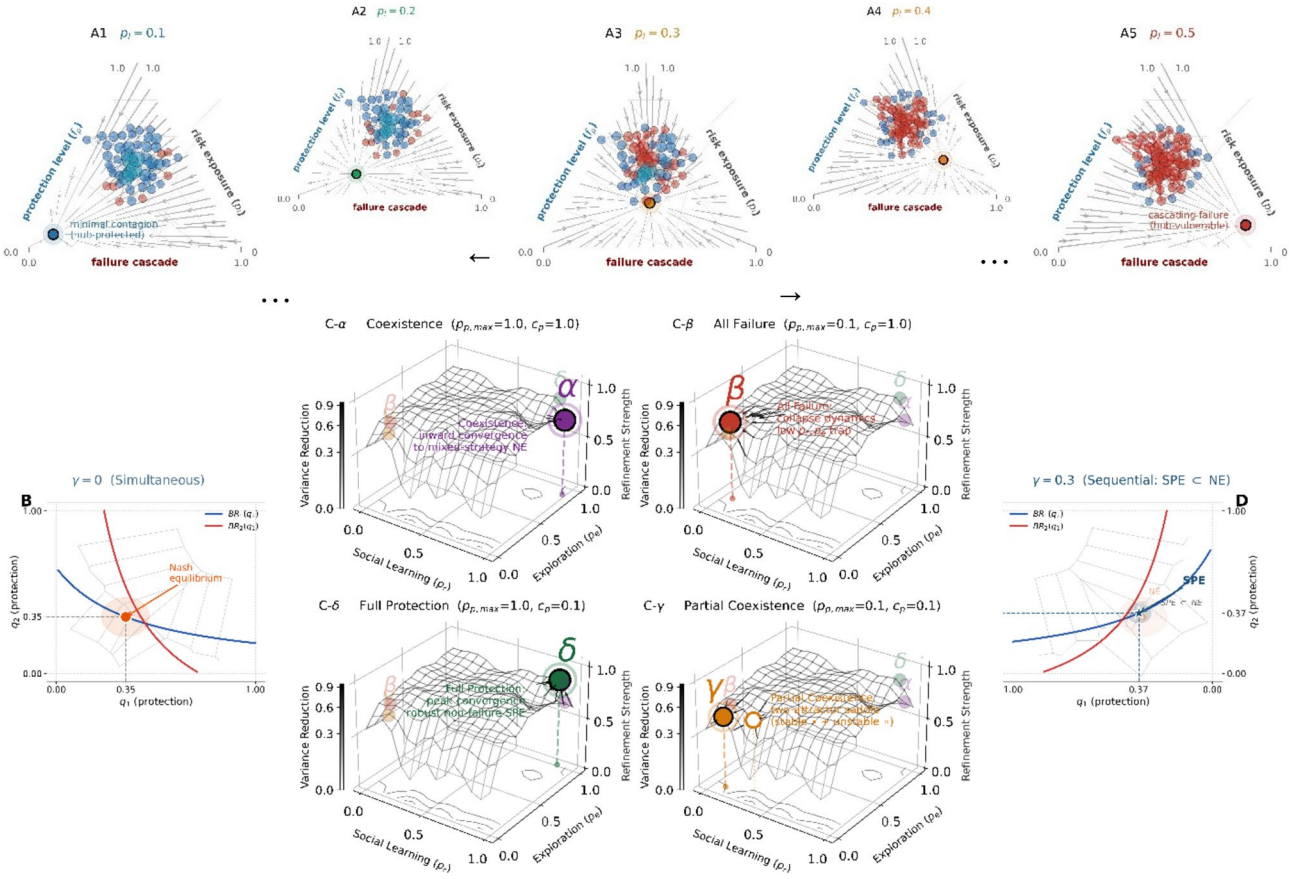

Fig. 3. Failure propagation and equilibrium refinement under sequential observation. (**A**) Progressive effect of neighbor-contagion risk on system composition, with ternary flow fields with embedded scale-free network states at p_l = 0.1, 0.2, 0.3, 0.4, and 0.5 (fixed γ = 0.3, p_{pmax} = 1.0, $c_{p,1/2}$ = 1.0). As p_l increases, the attractor shifts from protection dominance (left, blue network with hub-protected topology) through a balanced mixed state (center) to failure cascade dominance (right, red network with cascading hub failures). Network node colors indicate functional (blue) versus failed (red) states; node sizes reflect eigenvector centrality. The full animated progression across continuous p_l is provided in SI Movie S1. (**B**) Best-response diagram under simultaneous play (γ = 0), showing the Nash equilibrium at the intersection of $\mathrm{BR}_1(q_2)$ and $BR_2(q_1)$. (**C**) Refinement landscape across the (p_r, p_e) parameter space at γ = 0.3 for each scenario, namely α (coexistence, inward convergence), β (all failure, collapse dynamics), γ (partial coexistence, two-attractor saddle with stable and unstable fixed points), and δ (full protection, peak convergence). Variance reduction quantifies how sequential observation tightens the strategy distribution relative to the simultaneous baseline. (**D**) Best-response diagram under sequential play (γ = 0.3) with reversed axis, showing the refined SPE and the faded NE reference from Panel B; the dashed arrow indicates SPE ⊂ NE refinement.

$$\int F_{seq}(x)\,dx \leq \int F_{sim}(x)\,dx \quad \forall\, y \tag{5b}$$

Equation 5a implies sequential play yields weakly higher protection regardless of risk attitude. Equation 5b implies preference by all risk-averse agents ($u'' < 0$). The formal development of these stochastic dominance criteria, including the mean-preserving spread characterization and the connection to Arrow-Pratt risk measures, is provided in SI Text S4. Figure 4B confirms this across all four scenarios. The sequential cumulative distribution function (CDF) consistently lies rightward of the simultaneous CDF. The Kolmogorov-Smirnov distance D_{ks} reaches 0.50 for scenario δ, with network insets at the maximum divergence point showing that sequential play preserves hub protection while simultaneous play permits peripheral failures (δ) or cascading hub collapse (β, γ). This dominance arises from centrality-dependent move-order effects (Fig. 4A). Hub nodes moving first invest substantially more under sequential play, driven by the observation term $\gamma \cdot O_i(t)$ (Eq. 15b), with the gradient decaying monotonically toward the periphery. The underlying information structure follows from the conditional probability:

$$p(A_2|A_1) = p(A_1 \cap A_2)/p(A_1) \tag{6}$$

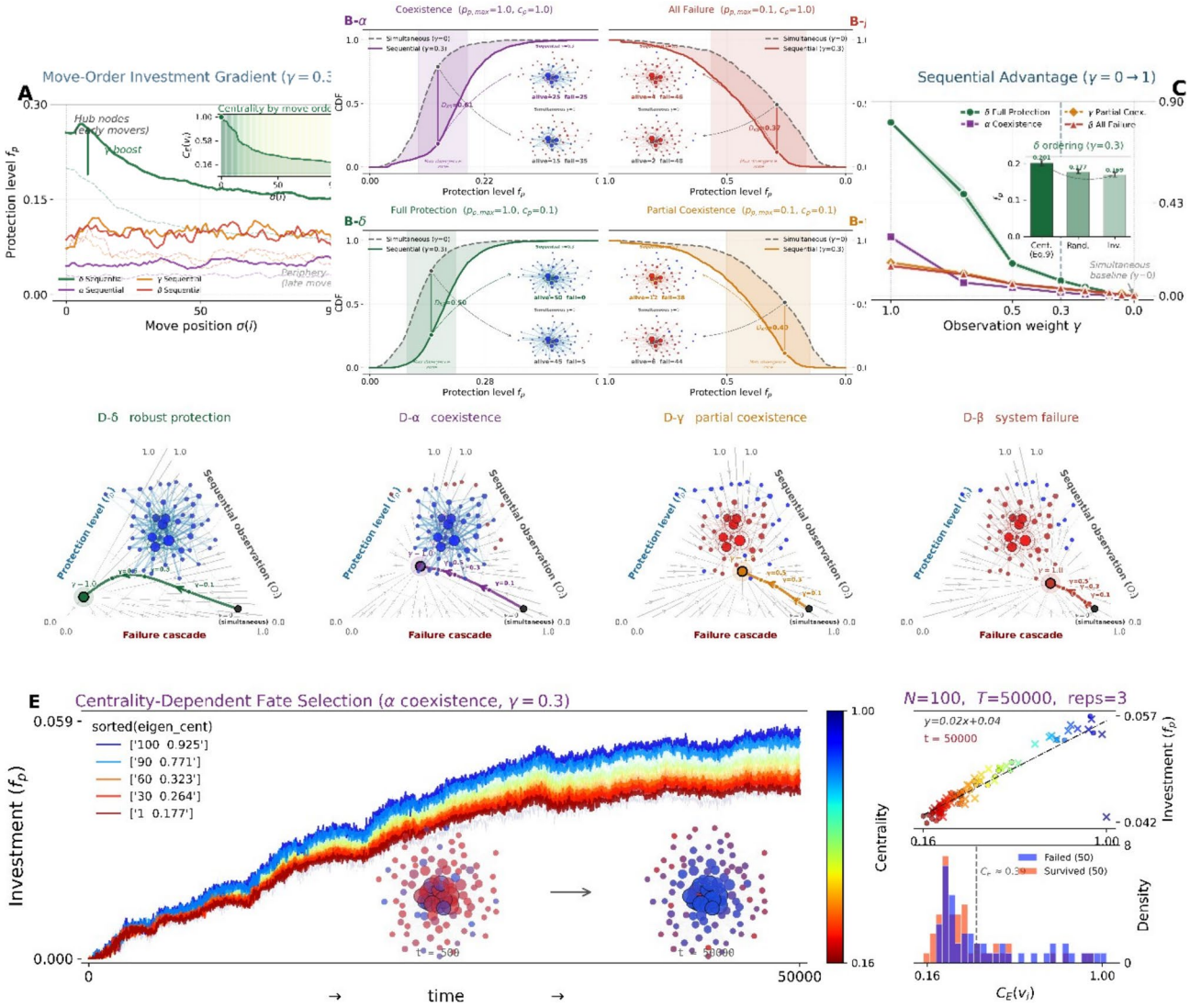

Fig. 4. Sequential dominance and ordering effects. (**A**) Move-order investment gradient showing protection level f_p as a function of move position $\sigma(i)$ under sequential ($\gamma = 0.3$, solid) and simultaneous ($\gamma = 0$, dashed) play. Hub nodes (early movers) invest more under sequential play, with the gradient most pronounced for scenario δ. Inset, eigenvector centrality profile colored by move order. (**B**) Cumulative distribution functions comparing sequential (colored solid) versus simultaneous (gray dashed) protection levels. Shaded regions indicate first-order stochastic dominance (Eq. 5a); the Kolmogorov–Smirnov distance D_{ks} marks maximum divergence. Paired network insets (upper = sequential, lower = simultaneous; blue = alive, red = failed) show topology-dependent failure patterns. For δ and α, peripheral nodes fail first; for γ and β, hub nodes fail first due to cascading exposure. (**C**) Protection gains Δf_p relative to the simultaneous baseline as a function of observation weight γ, confirming the $\gamma = 0$ reduction condition. Scenario δ exhibits the steepest gain. Inset: centrality-based ordering outperforms random and inverse orderings. (**D**) Attractor trajectory ternaries for each scenario showing equilibrium migration across $\gamma = 0 \rightarrow 1.0$ in a space defined by protection level (f_p), failure cascade, and sequential observation (O_i). All scenarios share the same $\gamma = 0$ baseline (simultaneous, failure-dominated), then diverge: δ sweeps to the protection vertex with complete network recovery; α reaches a mixed-strategy attractor; γ shows limited improvement with persistent hub failure; β barely migrates, confirming that sequential observation cannot rescue structurally constrained systems. Full 5-step ternary progressions are provided in SI Fig. S1 (The animated attractor migration for all four scenarios is provided in SI Movie S2). (**E**) Centrality-dependent fate selection (α coexistence, $\gamma = 0.3$, $N = 100$, $t = 50{,}000$, 3 replications). Left: f_p time-series stratified by eigenvector centrality C_E; representative traces colored by sorted centrality rank; embedded BA networks show failure→protection transition ($t = 500 \rightarrow t = 50{,}000$). Right: C_E– f_p regression ($R^2 = 0.817$, $p < 10^{-37}$) with logistic survival threshold ($C_E \approx 0.39$); histogram shows centrality distributions of failed (50) and survived (50) nodes.

When predecessor actions are independent, $p(A_1 \cap A_2) = p(A_1)\,p(A_2)$, observation provides no information and the game reduces to simultaneous play. Correlated strategies among networked agents break this independence, creating informational asymmetries that $O_i(t)$ aggregates as a sufficient statistic (SI Text S5). The sequential advantage scales monotonically with γ (Fig. 4C). At $\gamma = 0$ the models are equivalent, confirming the reduction condition (Proposition 2a). Centrality-based ordering amplifies the effect relative to random or inverse orderings (Fig. 4C inset). Figure 4D visualizes this transition through attractor trajectory ternaries, showing progressive equilibrium migration from the simultaneous-equivalent baseline (failure-dominated) toward scenario-specific attractors as γ increases from 0 to 1.0 (SI Movies S1 and S2). To verify that these macro-level ordering effects operate at the individual node level, Fig. 4E tracks strategy evolution within the α coexistence scenario ($c = 1 + (1 - f_m - f_p)\,c$, t = 50,000). Protection investment f_p stratifies by eigenvector centrality through the heuristic $f_p i = s_0, i + s_1, i C_E(v_i) + \gamma \cdot O_i(t)$, confirmed by regression (R^2 = 0.817, $p < 10^{-37}$). A centrality survival threshold emerges at $C_E \approx 0.39$, where nodes above this threshold accumulate sufficient functional capacity through sustained investment to maintain viability, while nodes below it lack the investment momentum to resist failure cascades. The sequential observation term $\gamma \cdot O_i(t)$ drives this stratification. Without it ($\gamma = 0$), no centrality-dependent differentiation arises. Embedded network snapshots confirm the failure → protection transition as the system evolves from t = 500 (failure-dominated) to t = 50,000 (protection equilibrium). This centrality-ordered structure is robust to network size. The four-scenario ordering and the relative position of the survival threshold persist on larger networks of N = 200 and N = 500, with the threshold's absolute value declining as the network grows (Section S7.6, Table S7, Fig. S3).

Having established that centrality-dependent mechanisms drive both population-level stochastic dominance (Fig. 4A–D) and individual-level investment stratification (Fig. 4E) within the model, we now examine whether analogous centrality–investment patterns appear in empirical networks across related domains.

Analogous centrality–investment patterns across simulated and empirical networks

The centrality-dependent fate selection observed in the simulated network (Fig. 4E) raises the question of whether scale-free systems with centrality-based decision ordering exhibit comparable investment stratification across domains. We now compare this pattern with empirical data, examining cross-domain centrality–protection correlation, the underlying scale-free topologies, and the form of the protection function across banking, epidemiology, and sports. In the sports setting that motivates the model, functional capacity $c_i(t)$ corresponds to a team or athlete performance measure, protection investment f_p to injury-prevention expenditure, eigenvector centrality C_E to an agent's interaction frequency within the team network, and the observation term $O_i(t)$ to what a later mover observes of more central predecessors' protection choices. The analogous correspondences for banking and epidemiology are given in SI Table S2. This mapping is stylized, since the model is intended to expose the centrality-ordered sequential mechanism rather than to serve as a direct empirical estimator, so the cross-domain calibration in Fig. 5 provides consistency evidence for a shared mechanism rather than a fitted prediction, as detailed in the Limitations.

Figure 5A examines cross-domain correspondence using empirical calibration from Park[24]. Under simultaneous play ($\gamma = 0$), centrality–protection correlations are r = 0.778 (banking, n = 127 G-SIBs), 0.825 (epidemiology, n = 43 OECD), and 0.694 (sports, n = 85 teams). Sequential observation ($\gamma = 0.3$) raises these to r = 0.906, 0.934, and 0.871 respectively (+16%, +13%, +26%), indicating that introducing the observation term $O_i(t)$ is associated with higher centrality–protection correlation across all three domains. Selection strengths cluster near s = 1 (banking 0.92 ± 0.12, epidemiology 1.08 ± 0.15, sports 1.01 ± 0.10), consistent with the bounded rationality calibration. Figure 5B presents the underlying scale-free topologies, namely a radial institutional hierarchy for banking, an organic contact network with dashed transmission links for epidemiology, and a position-differentiated team structure with traffic-light centrality coloring for sports. All three exhibit power-law centrality decay, indicating that the protection heuristic $f_p = f_p 0 + f_p 1 C_E$ operates on empirically grounded architectures.

The hyperbolic protection function $pp = p_{pmax}/(1 + c_{p,\frac{1}{2}}/(f_p c))$ provides a closer fit than logistic, linear, and exponential alternatives across all three empirical domains (Fig. 5C). The violin distributions in the upper panel show domain-specific patterns. Sports exhibits the widest R^2 gap between hyperbolic (0.926) and alternatives (0.389–0.451), indicating strong functional form sensitivity, while epidemiology shows a narrow range (0.557–0.643), suggesting that centrality–protection coupling in contact networks is less dependent on functional specification. Banking falls intermediate (0.483–0.783). The sequential model's hyperbolic R^2 = 0.803 is consistent with the empirical domain values (SI Text S6, Table S4). The lollipop comparison in the lower panel resolves R^2 by individual functional form, showing that hyperbolic achieves the highest R^2 for sports and banking while logistic marginally outperforms for epidemiology (0.643 vs. 0.603). This cross-domain comparison also addresses Ferrall and Smith's[8] finding of negligible strategic effects ($r \approx 0$) in 168 championship series under their dyadic treatment. Our multi-agent network extension detects centrality-dependent effects (linear R^2 = 0.817, Fig. 4E) absent from two-team models, indicating that network topology, not sequential structure alone, generates the dynamics that the dyadic treatment could not capture (SI Text S7, Table S5).

Discussion

This study extends bounded rationality game theory from simultaneous to sequential structures on scale-free networks, producing three principal findings. First, modified backward induction under bounded rationality yields ϵ-subgame perfect equilibria that converge to exact SPE as the rationality parameter β increases (SI Text S2), and these equilibria form refined subsets of Nash equilibria (SPE(Γ) $\subseteq$ NE(Γ)), with the refinement strength controlled by the observation weight γ. Second, in all four equilibrium scenarios examined, the sequential protection distribution under centrality-based decision ordering first-order stochastically dominates

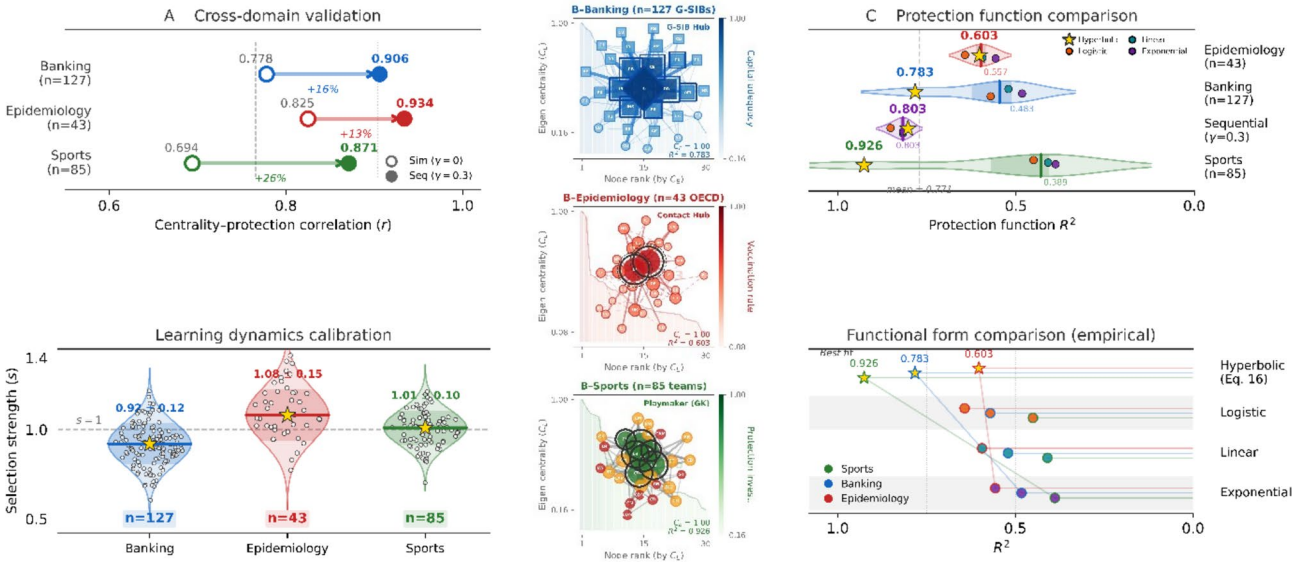

Fig. 5. Analogous centrality–investment patterns across simulated and empirical networks. (**A**) Cross-domain centrality–protection correlation. Simultaneous ($\gamma = 0$, open circles) → sequential ($\gamma = 0.3$, filled circles). Banking: 0.778→0.906 (+16%); epidemiology: 0.825→0.934 (+13%); sports: 0.694→0.871 (+26%). Lower panel: selection strength $s \approx 1$ across domains with n-case scatter (banking 127, epidemiology 43, sports 85), confirming bounded rationality calibration. Data from Park[24]. (**B**) Cross-domain scale-free topologies with C_E distributions (background) and colorbars indicating domain-specific protection proxies. Banking: radial G-SIB institutional hierarchy ($n = 127$). Epidemiology: dashed organic contact network with country-coded nodes ($n = 43$ OECD). Sports: traffic-light position-labeled team network ($n = 85$). BA networks, $N = 30$. (**C**) Protection function R^2 comparison. Upper panel: violin distributions showing R^2 range across four functional forms (hyperbolic, logistic, linear, exponential) per domain; yellow stars mark hyperbolic best-fit; form-colored circles (orange = logistic, teal = linear, purple = exponential) show individual R^2 values within each violin; sequential model R^2: hyperbolic 0.803, logistic 0.852, linear 0.817, exponential 0.817; logistic achieves the highest fit among functional forms. Lower panel: lollipop chart resolving R^2 by functional form across three empirical domains; hyperbolic achieves highest R^2 for sports (0.926) and banking (0.783); logistic marginally leads for epidemiology (0.643 vs. 0.603). Dashed line: empirical hyperbolic mean (0.771). See SI Text S6–S7 for data sources and Ferrall–Smith comparison.

the simultaneous baseline (Fig. 4A–D). Third, the centrality–investment relationship seen in the simulated network (Fig. 4E) also appears across the empirical domains examined, where sequential observation improves the correlation fits by 13–26% relative to the simultaneous baseline (Fig. 5A).

SPE emergence through bounded-rationality backward induction

The SPE $\subseteq$ NE inclusion, established within the extensive form structure[15,16] and resting on the Nash existence proved through Kakutani's fixed point theorem[13], suggests theoretical continuity with the simultaneous NE existence established in our earlier work[5]. The refinement operates through a mechanism distinct from classical backward induction. Softmax action selection[21,22] combined with social learning and exploration[19,20] produces ϵ -SPE that converge to exact SPE as the rationality parameter β increases (SI Text S2). The convergence rate scales as $T_{conv} = \mathrm{O}\left(\beta \log(\Delta(0)/\Delta_{ss})\right)$, with social learning (p_r) accelerating and exploration (p_e) bounding the steady-state neighborhood (SI Text S2, Eqs. S26–S30). This convergence property distinguishes our approach from cognitive hierarchy models[23], which require prior specification of reasoning depths, and from strategic stability refinements[25] that impose axiomatic restrictions on equilibrium selection rather than deriving refinement endogenously from sequential observation. Standard evolutionary dynamics on networks[26] and iterated multiplayer games under asynchronous best-response dynamics[27] lack the sequential observation channel that drives refinement in our model. The finding that sequential observation cannot rescue structurally constrained systems (scenario β, Fig. 4D) is consistent with results on strategic investment in networked systems[28], where protection capacity bounds constrain equilibrium outcomes regardless of information availability, and with broader game-theoretic principles of sequential rationality[29].

Centrality-based ordering and equilibrium selection

The centrality-based ordering creates a temporal structure with functional parallels to spatial organization in cyclic dominance games[30]. In rock-paper-scissors dynamics on complex networks, spatial heterogeneity sustains biodiversity through spiral waves and defensive alliances. Our $\sigma(i)$ ordering sustains equilibrium differentiation through an analogous mechanism, giving hub nodes a first-mover commitment advantage while peripheral nodes exploit observational information (Fig. 4A; SI Fig. S1). This specialization resonates with evidence that evolutionary dynamics produce role differentiation in strategic communities[31] and that coevolutionary feedback

between strategies and structure shapes equilibrium selection[26,32]. The sports parallel is concrete. Playmakers occupy high-centrality positions and constrain teammates' subsequent choices[14], athletes in multi-agent motor interactions converge to Nash equilibria through adaptive control[33], cycling leaders set pacing that followers accommodate[34], and first-mover tactical innovations cascade through team hierarchies[7].

The survival threshold in Fig. 4E gives individual-level confirmation of the ordering advantage. Nodes above $C_E \approx 0.39$ invest more through the sequential observation mechanism and accumulate capacity sufficient to resist failure cascades, while nodes below it lack the sustained investment to remain viable. This parallels the "too central to fail" logic in financial networks, where systemically important institutions hold higher capital buffers because their structural prominence demands greater protection[24,35]. In our model the same mechanism operates endogenously, where high-centrality nodes, acting as early movers, commit to higher protection that later movers observe and partially emulate, producing the dominance in Fig. 4B. Such centrality-dependent protection intensifies under multilayer coupling[36], consistent with the investment gradient steepening with connectivity. The protection function (Fig. 5C) follows a hyperbolic form across domains, outperforming alternatives for sports ($R^2 = 0.926$) and banking ($R^2 = 0.783$), while the sequential model shows a marginally better logistic fit ($R^2 = 0.852$ vs. hyperbolic 0.803), consistent with the sharper threshold in Fig. 4E, and epidemiology is competitive across all forms.

The model also connects abstract risk attitudes to operational bounded rationality. The softmax parameter β controls the effective curvature of the utility response, with high β approximating risk-averse behavior that favors known high-payoff actions (concave u, $u'' < 0$) and low β producing risk-seeking exploration (convex u, $u'' > 0$)[17,18]. This connection between classical risk theory and operational rationality (SI Text S3) supplies a bridge that standard behavioral game-theoretic treatments[37] identified as essential but did not formalize for network settings. Penalty-shootout goalkeepers show systematic action bias rather than optimal mixed play[38], and field studies of soccer players confirm departures from minimax predictions[39], consistent with the bounded rationality our β parameter captures. The resource-rational perspective[40] supports this reading, framing bounded rationality as an adaptive response to computational limits rather than a deficiency.

Behavioral regimes and sports-oriented dynamics

Beyond their role as mechanism parameters, the social learning rate p_r and the exploration rate p_e define a behavioral regime that governs how protection investment distributes across the network[5,19,20]. This pairing of imitation and exploration acts as an adaptive strategy update rule, and recent analysis of such rules in social dilemmas finds that the revision rule shapes the population outcome as strongly as the payoffs do[41]. Related work on networked evolutionary dynamics shows that self-interaction learning, where an agent weighs its own prior strategy, acts as a selection amplifier biasing which equilibrium the population reaches[42].

When both parameters are low, peripheral agents update and explore rarely, so investment concentrates among the early-moving hubs and the system settles into a monopolistic configuration where a few high-centrality nodes dominate the protection landscape. When both are high, peripheral agents update and explore actively, and investment spreads across a broader segment of the population, producing a distributed configuration in which the centrality gradient is preserved but flattened. This positions p_r and p_e as regime indices rather than auxiliary settings, since within the same topology and scenario class their choice determines whether the equilibrium is winner-takes-all or more egalitarian, even with the centrality ordering and protection capacity held constant. The regime view also explains why the variance reduction in Fig. 3C strengthens with higher (p_r , p_e), since the same parameters that flatten the investment distribution also tighten the strategy distribution around the SPE.

This regime view connects to a recurrent feature of professional sports markets, where rewards and visibility are heavy-tailed and a few star players or teams capture a disproportionate share of attention and resources[9,10]. Read through the bounded-rationality model, this winner-takes-all pattern corresponds to the low-(p_r, p_e) regime, where limited learning and exploration leave hubs structurally favored and the path from peripheral to central position narrows. Increasing (p_r, p_e) widens that path, as peripheral agents revise and explore more and accumulate the conditions under which their investment can approach that of the early movers. The model thus accounts for how a sports market migrates between monopolistic and distributed configurations as the institutional setting changes the rates at which workers learn from one another and explore alternative team affiliations. Worker mobility across teams, modeled as repeated participation in a sequence of stage games rather than a one-shot decision[8], is the empirical channel through which (p_r, p_e) act, since a player who switches teams samples additional decision contexts and operates closer to the high-(p_r, p_e) end of the regime axis. The boundary between the two configurations corresponds to where the early-mover and late-mover best-response curves intersect at the SPE, and its position shifts with (p_r, p_e) and the observation weight γ , as the Fig. 6 schematic makes explicit.

Read together, the panels formalize the preceding argument by anchoring the schematic in an empirical reference. Figure 6 Panel A documents the hub–periphery structure of an actual competitive network, where the eigenvector centrality profile, the multilayer topology, the sequential game progression, and the σ -ordered adjacency matrix establish that the centrality ordering used in the model is observable in real sports data. On this substrate, γ refines the equilibrium locally (Fig. 6 Panel B-left), (p_r, p_e) sets the regime configuration at the population level (Fig. 6 Panel B-middle), and the heavy-tailed and flatter distributional shapes (Fig. 6 Panel B-right) give that reading its qualitative signature. The empirical centrality structure thus returns in the contrast between hub-dominated and broadly connected topologies, the same contrast recurring across the empirical domains examined below, so the two regime axes operate at different scales rather than as alternative mechanisms.

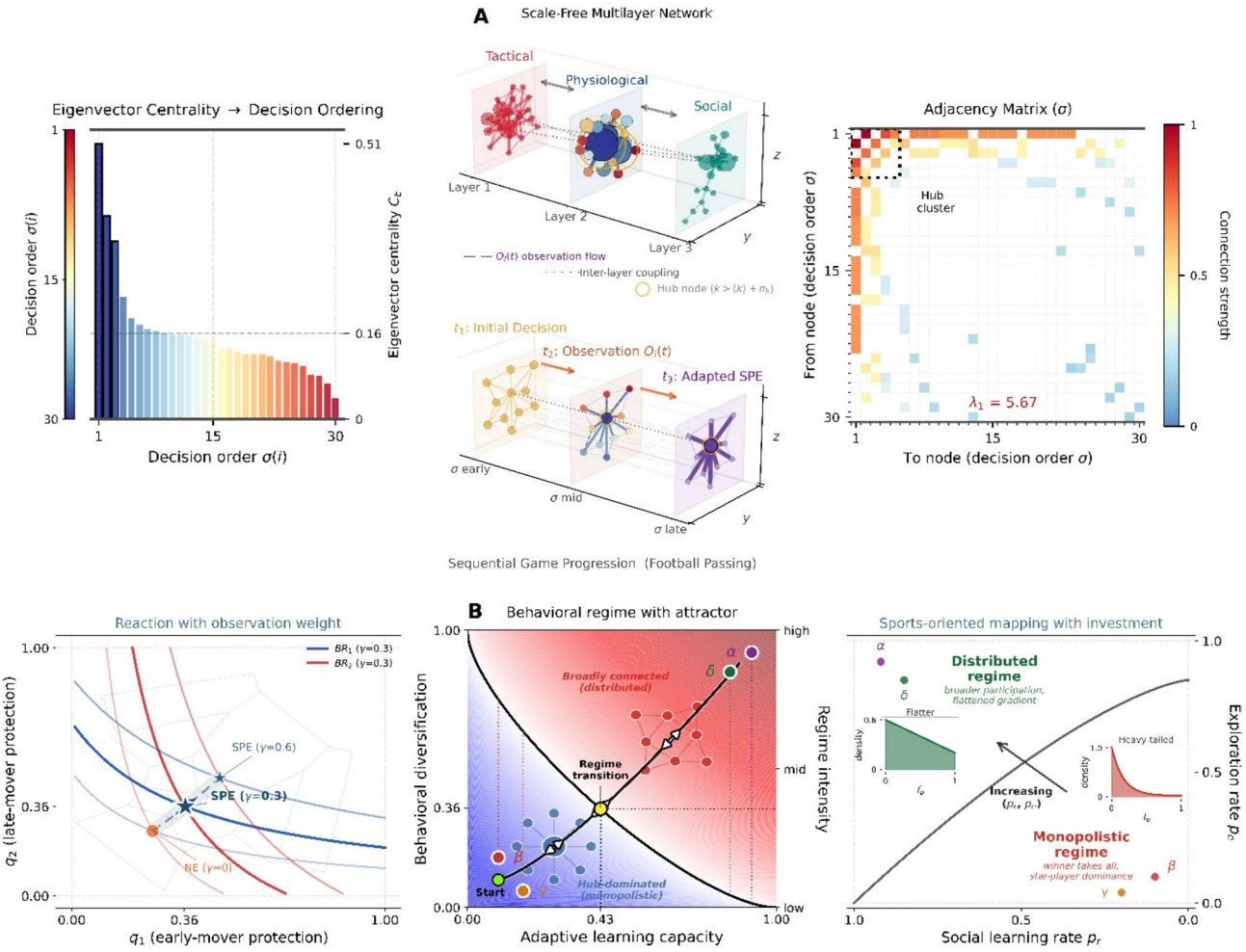

Fig. 6. Behavioral regimes and sports-oriented dynamics. (**A**) Empirical football network ($n = 11$; Grund[14], eigenvector centrality C_E profile with scale-free multilayer topology (Tactical, Physiological, Social layers), sequential game progression schematic, and σ -ordered adjacency matrix showing hub-cluster structure (CAM: $C_E = 0.49$, dominant eigenvalue $\lambda 1 = 5.67$). (**B**-left) Reaction-curve geometry for early-mover and late-mover protection q_1 and q_2 at three observation weights $\gamma \in \{0, 0.3, 0.6\}$. The orange marker at $\gamma = 0$ reproduces the simultaneous baseline[5]; dark-blue stars at $\gamma = 0.3$ and $\gamma = 0.6$ mark the SPE under bounded rationality. The dashed band traces the boundary locus along which the equilibrium migrates as γ increases. (**B**-middle) Behavioral regime field in the (p_r, p_e) plane. The seismic colormap separates monopolistic and distributed configurations along a single boundary curve. The yellow marker locates a regime transition along a representative parameter path, with bidirectional arrows indicating that traversal in either direction is accessible under parameter variation. Embedded network sketches express the qualitative connectivity of each side, and scenario anchors α , β , γ , δ sit at canonical (p_r, p_e) positions used throughout the manuscript. (**B**-right) Sports-oriented mapping with investment shapes. The same (p_r, p_e) plane is rendered with p_r reading right-to-left, with insets showing the qualitative shape of the protection-investment distribution f_p in each regime.

Cross-domain applications

The system-of-systems perspective advanced by Hochrainer-Stigler et al.[43] provides a natural interpretive context for our cross-domain findings. The first resilience dividend, avoided losses through protection investment, maps onto within-scenario equilibrium dynamics (Fig. 2), while the observation weight γ in Eq. 15a captures how sequential information flow generates second-order dividends through cross-agent coordination. Although the present model holds the network fixed, its protection dynamics relate to evolutionary dynamics on time-varying networks, where power-law activation patterns shape which strategies fixate[44] and bursty switching of activity can drive the collapse of network topologies[45]. Knowledge transfer across organizational boundaries[46] operates through a mechanism analogous to the centrality-weighted observation term $O_i(t)$. Agents with bridging positions in the network facilitate information flow that accelerates convergence to equilibrium. For financial stability, centrality-based ordering (Eq. 9) offers a principled mechanism for sequencing regulatory intervention, where globally systemically important banks act as early movers whose capital adequacy decisions constrain subsequent responses by smaller institutions[24]. Read as a multi-agent system, sequenced capital requirements

operate as a dynamic sanctioning mechanism that holds cooperative behavior in place across agents of differing size[47]. For public health crisis response, the conditional probability structure (Eq. 6) governs how later-responding units update vaccination or containment strategies based on predecessors' observed outcomes, consistent with the evolutionary dynamics governing biological cooperation under selection pressure[48]. Because containment is a public good, this setting also connects to the coevolution of population strategies and institutional rewards, where incentive structures and individual choices adjust to each other over the course of the response[49].

The present empirical validation, drawing on cross-domain calibration data analysis[8,24], confirms that network topology generates strategic differentiation invisible to two-team models. This finding motivates a structured empirical program targeting three sports contexts. Penalty shootout sequences, where kickers and goalkeepers adjust strategies based on observed earlier outcomes[38,39], provide a natural test of the observation mechanism. NFL draft order and batting lineup construction present sequential optimization contexts where evidence of departures from optimal play[50] maps directly onto the $\sigma\ (i)$ ordering. Each setting features a determinate decision order, observable predecessor actions, and centrality-differentiated strategic roles.

Limitations and future directions

Several boundaries of the present analysis should be stated clearly. The decision ordering is fixed and based on static eigenvector centrality, whereas in real systems the network structure and the centrality ranking co-evolve with the game dynamics, so the ordering used here is a snapshot rather than a fully dynamic schedule. All agents share a common rationality parameter β, whereas real populations exhibit heterogeneous strategic sophistication[23,37], so the present results describe a homogeneous-rationality regime. The observation term $O_i\ (t)$ assumes accurate perception of predecessors' actions and omits the noise and partial observability that characterize many real strategic settings[15]. A sensitivity analysis that adds noise to the observed predecessor protection shows that the stochastic dominance and the survival threshold persist across the noise range, while the graded centrality-investment correlation weakens once the noise reaches a moderate level (SI Text S7.5, SI Fig. S2).

A second set of boundaries concerns empirical scope. Although the main analyses use a fixed network size, the four-scenario ordering and the relative position of the centrality survival threshold hold across networks from N = 100 to N = 500. The linear coefficient between node centrality and protection investment declines as the network grows, because max-normalized eigenvector centrality concentrates toward zero at larger N and compresses the range of the predictor, so the linear value reported here applies to N = 100 while the rank ordering it summarizes persists across sizes (Section S7.6). The empirical calibration treats the model as a stylized representation of each domain rather than a fitted predictor, so the cross-domain correspondence in Fig. 5 and SI Table S2 is consistency evidence for a shared mechanism and not a direct empirical estimate.

Future extensions include dynamic ordering that co-evolves with the game state, agent-specific β_i distributions calibrated to empirical behavioral data[22], evolutionary games on higher-order structures such as simplicial[51], and expanded multilayer network representations that explicitly couple tactical, physiological, and social interaction layers. The zero-sum assumption could be relaxed to incorporate cooperative elements observed in team sports, where partial cooperation coexists with inter-team competition[5,48].

Methods

Network construction and agent representation

The network topology follows the Barabási–Albert preferential attachment model[52], generating scale-free networks with N nodes and average connectivity m, where new nodes attach with probability proportional to degree to produce the power-law degree distribution characteristic of sports interaction networks[1,4,5]. This topology is appropriate for two structural reasons. First, sports networks form multilayer coupled systems, where a tactical decision layer, a physiological performance layer, and a social coordination layer share the same nodes but follow layer-specific dynamics, so that localized disruptions propagate more aggressively than in single-layer systems, following power-law scaling that accelerates failure transmission across layers (Fig. 6A). Second, empirical team passing networks, player interaction patterns, and coaching hierarchies show heavy-tailed degree distributions[1,4,53], in which a few highly connected hub nodes disproportionately influence system-wide outcomes. Each node is a sports agent with functional capacity $c_i\ (t)$ representing performance capacity, strategy parameters (s_i^0, s_i^1) determining protection investment, and network position characterized by eigenvector centrality. The adjacency matrix and eigenvector centrality are defined as:

$$A = (a_{ij}),\ where\ a_{ij} = 1\ if\ edge\ exists\ between\ i\ and\ j,\ and\ 0\ otherwise \tag{7}$$

$$C_E\ (v_i) = \lambda_1^{-1} \sum_{j=1} N\ a_{ij}\ e_j \tag{8}$$

where e_j is the eigenvector value of node j and λ_1 is the dominant eigenvalue characterizing the asymptotic rate of pathway proliferation through the network[54,55]. The complete derivation of the Kakutani fixed point conditions for this network game is provided in SI Text S1.

Sequential game formalization

Definition 1 An extensive form game Γ consists of a set of players $N = \{1,2,\ldots,n\}$, a game tree T with root node r, decision nodes D_i for each player i, and terminal nodes Z, action sets $A\ (d)$ at each decision node, information sets H_i partitioning decision nodes for player i, and payoff function u_i: $Z \to \mathbb{R}$ for each player. Because agent $\sigma\ (k)$ observes the realized actions of all predecessors $\sigma\ (1),\ldots\ \sigma\ (k-1)$ before choosing,

every decision node constitutes a singleton information set, making the game one of perfect information admitting backward induction[15,16]. This modeling choice is motivated by sports contexts where tactical decisions are publicly observable[38].

Decision ordering in sports networks

Network topology determines the natural decision sequence. High-centrality nodes act as strategic initiators (early movers), while peripheral nodes serve as tactical adapters (late movers). The decision order function is:

$$\sigma : N \to \{1,2,\ldots,n\} \tag{9}$$

where $\sigma(i)$ denotes the position of agent i in the decision sequence, determined by:

$$\sigma(i) \propto f(C_E(v_i), degree(i), context) \tag{10}$$

In the default specification, agents are ranked in descending order of eigenvector centrality, so that the most central node decides first. This ordering captures how centrally positioned players set strategic directions constraining peripheral agents' tactical choices[14].

Backward induction mechanism

Standard backward induction identifies the subgame perfect equilibrium by iterating from terminal nodes to the root[15,56]. We modify this procedure through probabilistic action selection. At each decision node assigned to player i, the probability of selecting action a is.

$$p_i(a|d) = \exp(\beta \cdot V_i(a)) / \sum_{a'} \exp\left(\beta \cdot V_i\left(a'\right)\right) \tag{11}$$

where β is the rationality intensity parameter ($\beta \to \infty$ recovers exact backward induction, and $\beta \to 0$ produces uniform random play) and $V_i(a)$ is the computed continuation value of action a. This formulation follows the quantal response equilibrium tradition[21,22]. The full decision rule integrates social learning, strategic exploration, and softmax backward induction through a sequential priority mechanism:

$$\widehat{a}(d) = a_j \ (imitation), \ a_{random}(exploration), \ or \ a_{computed} \ (softmax) \tag{12}$$

The three cases in Eq. 12 apply with probability p_r for imitation, ($1 - p_r$) p_e for exploration, and ($1 - p_r$) ($1 - p_e$) for softmax selection. At each time step, agent i first attempts imitation with probability p_r, where a neighbor j is selected at random and agent i copies j's action if $\pi_{ij} \geq U$, where $U \sim$ Uniform [0,1] and π_{ij} is the imitation probability based on the functional capacity differential (Eq. 13). If imitation does not occur, agent i explores with probability p_e by selecting an action uniformly at random from A_i. If neither imitation nor exploration occurs, agent i applies the softmax rule (Eq. 11) with probability $(1 - p_r)(1 - p_e)$. The imitation probability is:

$$\pi(c_j, c_i) = 1/(1 + \exp(-s \cdot (c_j, c_i))) \tag{13}$$

This sequential priority structure guarantees that the three cases are mutually exclusive regardless of parameter values. The design matches the published simultaneous model[5], where the same priority ordering governs strategy updating at each time step.

Protection mechanism in sequential structure

Functional capacity $c_i(t)$ represents each node's performance capacity, following the notation of the published simultaneous model[5,6]. Each node i possesses functional capacity updated at each time step as:

$$c_i(t+1) = [1 + (1 - f_m - f_p)] \cdot c_i(t) \tag{14}$$

where f_m is the maintenance cost and f_p is the protection investment. In the sequential model, the protection investment incorporates an observation term:

$$f_p^i(t) = s_i^0 + s_i^1 \cdot C_E(v_i) + \gamma \cdot O_i(t) \tag{15a}$$

where $O_i(t)$ is the centrality-weighted mean of predecessors' protection levels:

$$O_i(t) = \sum_{j:\sigma(j)<\sigma(i)} w_i \cdot f_p^i(t) \Big/ \sum_{j:\sigma(j)<\sigma(i)} w_i \tag{15b}$$

with weights $w_i = C_E(v_i)$, protection decisions by high-centrality predecessors exert proportionally greater influence on later movers. For the first mover ($\sigma(i) = 1$), the predecessor set is empty and $O_i(t) = 0$, reducing the first mover's protection to the simultaneous form. The formal proof that $O_i(t)$ serves as a sufficient statistic for the payoff-relevant history, compressing the exponential history space to constant dimension, is given in SI Text S5. The coefficient $\gamma \geq 0$ controls the sensitivity of later movers to observed predecessor behavior. When $\gamma = 0$, Eq. 15a reduces exactly to the published simultaneous form $f_p^i = s_i^0 + s_i^1 \cdot C_E(v_i)$[5]. The protection probability follows:

$$p_p = p_{p\max}/(1 + c_{p,\frac{1}{2}}/(f_p \cdot c)) \tag{16}$$

Nodes fail with baseline probability p_n or through neighbor-propagated risk with probability p_l. Upon failure, functional capacity is reset to zero. These mechanisms are preserved exactly from the simultaneous model to ensure direct comparability. The stochastic dominance criteria used to compare sequential and simultaneous protection distributions (Eq. 5a, 5b) are formally developed in SI Text S4, including the mean-preserving spread characterization. In simultaneous-game recovery, when $\gamma = 0$, Eq. 15a reduces to this simultaneous form, eliminating all dependence on predecessors' actions. Because $O_i(t) = 0$ for every agent, no decision node's payoff depends on other agents' actions within the same time step. The sequential ordering σ becomes strategically irrelevant and SPE coincides with NE, guaranteeing exact reproducibility of the published simultaneous model[5] as the special case $\gamma = 0$.

Subgame perfect equilibrium characterization

Definition 2 A strategy profile $s^*$is an SPE if it constitutes a Nash equilibrium in every subgame Γ' of Γ:

$$u_i(s_i^*, s_{-i}^* | \Gamma') \geq u_i\left(s_i', s_{-i}^* \middle| \Gamma'\right), \forall s_i' \in S_i\left(\Gamma'\right) \tag{17}$$

Theorem 1 Every subgame perfect equilibrium is a Nash equilibrium, but not every Nash equilibrium is subgame perfect:

$$SPE(\Gamma) \subseteq NE(\Gamma) \tag{18}$$

This relationship provides theoretical continuity with our published results[5]. The refinement eliminates NE sustained by non-credible threats[16,56]. The inclusion is proved for the centrality-ordered sequential game in SI Text S2, where the observation term $O_i(t)$ is the channel through which subgame optimality removes those non-credible responses. The complete Kakutani fixed point derivation is provided in SI Text S1.

Proposition 1 Under softmax action selection (Eq. 11) with rationality parameter $\beta > 0$, an ϵ -SPE exists with $\epsilon = O(1/\beta)$, converging to exact SPE as $\beta \to \infty$ (SI Text S2).

Proposition 2 When $\gamma = 0$, sequential play produces $SPE(\Gamma) = NE(\Gamma)$. When $\gamma > 0$ with heterogeneous centrality, sequential play produces $SPE(\Gamma) \subset NE(\Gamma)$, with refinement strength increasing in γ and in the variance of the centrality distribution (SI Text S2).

Proposition 2a At $\gamma = 0$, $O_i(t) = 0$ for every agent and Eq. 15a reduces exactly to the published simultaneous protection function, so the sequential game is strategically equivalent to the simultaneous model and reproduces its equilibrium results[5].

Empirical validation methodology

Cross-domain validation (Fig. 5) uses calibration data from Park[24], namely banking (n = 127 G-SIBs, BIS Basel III, 2015–2024), epidemiology (n = 43 OECD, WHO/OWID, 2020–2023), and sports (n = 85 teams, UEFA FFP/NFL health-safety, 2015–2019). Data sources, variable mappings, and protection function comparisons are documented in SI Text S6 (Tables S1–S5). The Ferrall and Smith[8] comparison draws on their maximum likelihood estimates from 168 championship series across baseball (n = 85), basketball (n = 43), and hockey (n = 40), with details in SI Text S7.

Simulation protocol

Simulations extend the published codebase[5]. Initialize the scale-free network ($N = 100$, $m = 5$), determine ordering σ by eigenvector centrality (Eq. 9), execute modified backward induction (Eqs. 11–13), update strategies, functional capacity, and protection (Eqs. 14–16), and iterate until equilibrium detection or maximum T. Four-scenario analysis (Figs. 2, 3 and 4) uses T = 100 with 50 replications, and centrality-dependent fate selection (Fig. 4E) uses T = 50,000 with 3 replications at p_e = 0.001. Simulation parameter details are documented in SI Text S7 (Table S6), code and data deposition details are reported in the Data availability section.

Data availability

The core simulation and analysis code is publicly available on GitHub (https://github.com/pcw8531/sequential-game-sports-networks) and archived on Zenodo. The release supporting this study is version v1.1.0 (https://doi.org/10.5281/zenodo.20830066), and the concept DOI (https://doi.org/10.5281/zenodo.19528356) always resolves to the latest version. All empirical calibration data used in this paper are derived from previously published sources and are listed alongside their original references in the manuscript. Detailed mappings to specific tables and figures are documented in Supplementary Information Section S6.

Received: 26 May 2026; Accepted: 13 July 2026
Published online: 29 July 2026

References

1. Wäsche, H., Dickson, G., Woll, A. & Brandes, U. Social network analysis in sport research: an emerging paradigm. *Eur. Sport Manag Q.* **17**, 103–131. https://doi.org/10.1080/16184742.2017.1356332 (2017).
2. Narizuka, T. & Yamazaki, Y. Science of team sports: network analysis of movement and interactions. *Eur. J. Sport Sci.* **18**, 911–919 (2018).
3. Jusup, M. et al. Social physics. *Phys. Rep.* **948**, 1–148. https://doi.org/10.1016/j.physrep.2021.10.005 (2022).
4. Park, C. Optimizing resilience in sports science through an integrated random network structure. *Sage Open* **15** (2026).
5. Park, C. & Fath, B. D. Bounded rationality produces Nash equilibria in sports networks: protection, learning, and strategic adaptation. *Phys. A* 131258 https://doi.org/10.1016/j.physa.2026.131258 (2026).
6. Seifert, L., Button, C. & Davids, K. Key properties of expert movement systems in sport. *Sports Med.* **43**, 167–178 (2014).
7. Newell, S. & Swan, J. The diffusion of innovations in sport organizations. *J. Sport Manag.* **9**, 317–337 (1996).
8. Ferrall, C. & Smith, A. A. Jr. A sequential game model of sports championship series: Theory and estimation. *Rev. Econ. Stat.* **81**, 704–719 (1999).
9. Rosen, S. Prizes and incentives in elimination tournaments. *Am. Econ. Rev.* **76**, 701–715 (1986).
10. Lazear, E. P. & Rosen, S. Rank-order tournaments as optimum labor contracts. *J. Polit. Econ.* **89**, 841–864 (1981).
11. von Neumann, J. & Morgenstern, O. *Theory of Games and Economic Behavior* (Princeton University Press, 1944).
12. Nash, J. F. Equilibrium points in n-person games. *Proc. Natl. Acad. Sci. U.S.A.* **36**, 48–49 (1950).
13. Kakutani, S. A generalization of Brouwer's fixed point theorem. *Duke Math. J.* **8**, 457–459 (1941).
14. Grund, T. U. Network structure and team performance: The case of English Premier League soccer teams. *Soc. Netw.* **34**, 682–690 (2012).
15. Kuhn, H. W. Extensive games and the problem of information. In *Contributions to the Theory of Games, Volume II* (eds Kuhn, H. W. & Tucker, A. W.) 193–216 (Princeton University Press, 1953).
16. Selten, R. Reexamination of the perfectness concept for equilibrium points in extensive games. *Int. J. Game Theory* **4**, 25–55 (1975).
17. Bernoulli, D. Exposition of a new theory on the measurement of risk. *Econometrica* **22**, 23–36 (1954).
18. Pratt, J. W. Risk aversion in the small and in the large. *Econometrica* **32**, 122–136 (1964).
19. Arthur, W. B. Designing economic agents that act like human agents: a behavioral approach to bounded rationality. *Am. Econ. Rev.* **81**, 353–359 (1991).
20. Simon, H. A. A behavioral model of rational choice. *Q. J. Econ.* **69**, 99–118 (1955).
21. McKelvey, R. D. & Palfrey, T. R. Quantal response equilibria for normal form games. *Games Econ. Behav.* **10**, 6–38 (1995).
22. McKelvey, R. D. & Palfrey, T. R. Quantal response equilibria for extensive form games. *Exp. Econ.* **1**, 9–41 (1998).
23. Camerer, C. F., Ho, T.-H. & Chong, J.-K. A cognitive hierarchy model of games. *Q. J. Econ.* **119**, 861–898 (2004).
24. Park, C. Network centrality drives optimal protection investment against systemic risk propagation in complex systems. *Sci. Rep.* **16**, 4595 (2026).
25. Kohlberg, E. & Mertens, J. F. On the strategic stability of equilibria. *Econometrica* **54**, 1003–1037 (1987).
26. Perc, M. & Szolnoki, A. Coevolutionary games: a mini review. *Biosystems* **99**, 109–125 (2010).
27. Zhu, Y., Xia, C. & Chen, Z. Nash equilibrium in iterated multiplayer games under asynchronous best-response dynamics. *IEEE Trans. Autom. Control.* **68**, 5798–5805 (2024).
28. Leduc, M. V. & Momot, R. Strategic investment in protection in networked systems. *Netw. Sci.* **5**, 108–139 (2018).
29. Dutta, P. K. *Strategies and Games: Theory and Practice* (MIT Press, 1999).
30. Szolnoki, A. et al. Cyclic dominance in evolutionary games: A review. *J. R. Soc. Interface* **11**20140735. (2014).
31. Jia, D. et al. Evolutionary dynamics drives role specialization in a community of players. *J. R. Soc. Interface* **17**20200174. (2020).
32. Sigmund, K. & Nowak, M. A. Evolutionary game theory. *Curr. Biol.* **9**, R503–R505 (1999).
33. Braun, D. A., Ortega, P. A. & Wolpert, D. M. Nash equilibria in multi-agent motor interactions. *PLoS Comput. Biol.* **5**, e1000468 (2009).
34. Atkinson, G., Davison, R., Jeukendrup, A. & Passfield, L. Science and cycling: Current knowledge and future directions for research. *J. Sports Sci.* **21**, 767–787 (2003).
35. Park, C. Network and agent dynamics with evolving protection against systemic risk. *Complexity* **2020**, 1–16 (2021).
36. Bianconi, G. et al. Complex systems in the spotlight: next steps after the 2021 Nobel Prize in Physics. *J. Phys. Complex.* **4** 010201. (2023).
37. Camerer, C. F. *Behavioral Game Theory: Experiments in Strategic Interaction* (Princeton University Press, 2003).
38. Bar-Eli, M., Azar, O. H., Ritov, I., Keidar-Levin, Y. & Schein, G. Action bias among elite soccer goalkeepers: the case of penalty kicks. *J. Econ. Psychol.* **28**, 606–621 (2007).
39. Azar, O. H. & Bar-Eli, M. Do soccer players play the mixed-strategy Nash equilibrium?. *Appl. Econ.* **43**, 3591–3601 (2011).
40. Lieder, F. & Griffiths, T. L. Resource-rational analysis: Understanding human cognition as the optimal use of limited computational resources. *Behav. Brain Sci.* **43**, e1 (2020).
41. Wang, L., Hua, S., Liu, Y., Liu, S. & Liu, L. Evolutionary dynamics of adaptive strategy update rules in social dilemmas. *Appl. Math. Model.* **155**, 116724. https://doi.org/10.1016/j.apm.2025.116724 (2025).
42. Zeng, Z., Feng, M. & Szolnoki, A. Evolutionary dynamics with self-interaction learning in networked systems. *IEEE Trans. Netw. Sci. Eng.* **13**, 296–313. https://doi.org/10.1109/TNSE.2025.3583016 (2025).
43. Hochrainer-Stigler, S. et al. Understanding multiple resilience dividends and system boundaries in disaster- and climate-risk management. *Environ. Res. Lett.* **20**, 044026 (2025).
44. Zeng, Z., Feng, M., Liu, P. & Kurths, J. Complex network modeling with power-law activating patterns and its evolutionary dynamics. *IEEE Trans. Syst. Man. Cybern Syst.* **55**, 2546–2559 (2025).
45. Zeng, Z., Feng, M., Perc, M. & Kurths, J. Bursty switching dynamics promotes the collapse of network topologies. *Proc. R. Soc. A* **481**, 20240936. https://doi.org/10.1098/rspa.2024.0936 (2025).
46. Tortoriello, M., Reagans, R. & McEvily, B. Bridging the knowledge gap: The influence of strong ties, network cohesion, and network range on the transfer of knowledge between organizational units. *Organization Science* **23**, 1024–1039 (2013).
47. Liu, L., Wang, L., Niu, W. & Hua, S. Dynamic sanctioning mechanism for cooperative multi-agent systems. *Expert Syst. Appl.* **296**, 128873. https://doi.org/10.1016/j.eswa.2025.128873 (2026).
48. Nowak, M. A. & Sigmund, K. Evolutionary dynamics of biological games. *Science* **303**, 793–799 (2004).
49. Hua, S. & Liu, L. Coevolutionary dynamics of population and institutional rewards in public goods games. *Expert Syst. Appl.* **237**, 121579. https://doi.org/10.1016/j.eswa.2023.121579 (2024).
50. Kovash, K. & Levitt, S. D. Professionals Do Not Play Minimax: Evidence from Major League Baseball and the National Football League. NBER Working Paper No. 15347 (National Bureau of Economic Research, 2010).
51. Guo, H. et al. Evolutionary games on simplicial complexes. *Chaos Solitons Fractals.* **150**, 111103 (2022).
52. Barabási, A.-L. & Albert, R. Emergence of scaling in random networks. *Science* **286**, 509–512 (1999).
53. Park, C. & Kim, S. Network-agent systems dynamic modelling: a guide for sport science. *Korean J. Sport Sci.* **31**, 514–533 (2021).
54. Borrett, S. R., Fath, B. D. & Patten, B. C. Functional integration of ecological networks through pathway proliferation. *J. Theor. Biol.* **245**, 98–111 (2008).
55. Borrett, S. R. & Patten, B. C. Structure of pathways in ecological networks: theoretical and empirical foundations. *Ecol. Model.* **170**, 173–184 (2004).
56. Osborne, M. J. & Rubinstein, A. *A Course in Game Theory* (MIT Press, 1994).

Author contributions

C.P. conceived and designed the study, developed the model, performed simulations, analyzed the data, conducted empirical validation, and wrote the manuscript.

Funding

This work was supported by the Basic Science Research Program through the National Research Foundation of Korea (NRF) funded by the Ministry of Education (Grant Number: 2020R1I1A1A01056967) and by Seoul National University BK21 Four Program.

Declarations

Competing interests

The author declares no competing interests.

Additional information

Supplementary Information The online version contains supplementary material available at https://doi.org/10.1038/s41598-026-62459-6.

Correspondence and requests for materials should be addressed to C.P.

Reprints and permissions information is available at www.nature.com/reprints.

Publisher's note Springer Nature remains neutral with regard to jurisdictional claims in published maps and institutional affiliations.

Open Access This article is licensed under a Creative Commons Attribution-NonCommercial-NoDerivatives 4.0 International License, which permits any non-commercial use, sharing, distribution and reproduction in any medium or format, as long as you give appropriate credit to the original author(s) and the source, provide a link to the Creative Commons licence, and indicate if you modified the licensed material. You do not have permission under this licence to share adapted material derived from this article or parts of it. The images or other third party material in this article are included in the article's Creative Commons licence, unless indicated otherwise in a credit line to the material. If material is not included in the article's Creative Commons licence and your intended use is not permitted by statutory regulation or exceeds the permitted use, you will need to obtain permission directly from the copyright holder. To view a copy of this licence, visit http://creativecommons.org/licenses/by-nc-nd/4.0/.

© The Author(s) 2026